UNIVERSITÀ DEGLI STUDI DI PADOVA

Dipartimento di Fisica e Astronomia "Galileo Galilei"
Dipartimento di Ingegneria dell'Informazione
Corso di Laurea in Fisica

Tesi di Laurea

Optimization of a Pulsed Source of Entangled Photons for the Violation of the "CHSH" Inequality

Relatore:
Prof. Giuseppe Vallone
Correlatore:
Dr. Francesco Vedovato

Laureando:
Federico De Bettin

Anno Accademico 2017/2018

Preface

This thesis focuses on my work carried out in the Quantum Communications laboratory by the Quantum Future research group of the Department of Information Engeneering, in which I worked on the creation and optimization of a pulsed source of polarization entangled photons. The main focus in the laboratory was to optimize the experimental setup to prove the entangled nature of the photons produced. This was done by violating the Bell inequality in the form presented by Clauser, Horne, Shimony and Holt (CHSH) in 1969. The present work's objective is to provide an overview of all the crucial physical phenomena exploited in the experiment to obtain the wanted results.

In section 1 a presentation of the phenomenon of entanglement and of Bell's argument proving the incapability to describe its properties with a both real and local theory is given, along with the derivation of the "CHSH" inequality and the possibility to violate it with polarization entangled photons. Sections 2 and 3 focus on the properties of the Gaussian beam used in the experiment and its source: the mode-locked Mira laser. A brief discussion about mode-locked lasers and their properties is provided. In section 4 the nonlinear optical phenomena of second harmonic generation and spontaneous parametric down conversion are discussed, the former from a classical standpoint and the latter with a few quantum mechanical considerations. Section 5 focuses on polarization optics and the both classical and quantum mechanical formalism of the Jones vectors. A discussion of the effects of the birefringent devices used in the experiment on the photons' state is provided. Finally, sections 6 and 7 display a complete overview of the experimental setup and the results obtained for the violation of the inequality. A systematic explanation of the experimental optimization procedure is provided in section 6 as it may be useful for the future experimenters, since it proved to be tricky.

Throughout all the work, various characteristics of the devices used in the experimental setup are given, hopefully making the most important and peculiar aspects of the experiment clear.

this page intentionally left balnk

Contents

this page intentionally left blank

1 Context

Some features of quantum mechanics are baffling and counterintuitive. Following the arguments given firstly by Einstein, Podolsky and Rosen and secondly by Bell and Clauser, Horne, Shimony and Holt, it is possible to show that a system of two particles describable by an *entangled* state exhibits properties that can not be described by a both *realistic* and *local* theory. In this section these arguments will be presented in the context of the experiment of interest.

1.1 The EPR paradox

The paper published by Einstein, Podolsky and Rosen in 1935 [1] raised a paradox within quantum mechanics, which took almost thirty years to be solved.
The key in the EPR argument is the introduction of correlated pure states of two particles, which in our case are photons, of the form

$$|\psi\rangle = N \sum\nolimits_n q_n \, |a_n\rangle_1 \otimes |b_n\rangle_2 \,, \tag{1.1}$$

where $\{|a_n\rangle_1\}$ and $\{|b_n\rangle_2\}$ are ortho-normal eigenstates for some operators A_1 and B_2 with eigenvalues $\{a_n\}$ and $\{b_n\}$ acting on particles 1 and 2 respectively, N is the normalization factor and $|q_n|^2 = p_n$ is the probability of the pair of eigenvalues (a_n, b_n) to be measured. The wave function of the system depends on both of the particles and it is not separable, meaning that

$$|\psi\rangle \neq |\chi\rangle_1 \otimes |\varphi\rangle_2 \,, \tag{1.2}$$

so that even if the particles get to be spatially separated, they are still correlated. Equation (1.2) is the actual formal definition of a pure *entangled state*. If the two particles are far from each other and a measure of A_1 is performed on particle 1 giving the eigenvalue a_n as the result, particle 1 must be in the state $|a_n\rangle_1$, while particle 2 must be in the state $|b_n\rangle_2$. This process is known as *wave packet reduction*. This way, the result of a measurement of B_2 on particle 2 will give the result b_n, which is the eigenvalue relative to $|b_n\rangle_2$, with certain probability.
The same procedure can be applied by writing

$$|\psi\rangle = N' \sum\nolimits_n q'_n \, |c_n\rangle_1 \otimes |d_n\rangle_2 \,, \tag{1.3}$$

where $\{|c_n\rangle_1\}$ and $\{|d_n\rangle_2\}$ are ortho-normal eigenstates for some operators C_1 and D_2 and by performing a measurement of C_1.
Hence, depending on the measured quantity related to particle 1, the wave function of particle 2 can be an eigenstate of different operators. This is shown to be possible even if the operators B_2 and D_2 do not commute, within quantum mechanics. EPR claims that for a physical theory to be *complete*, the condition of completeness *" every element of the physical reality must have a counterpart in the physical theory"* has to be satisfied. In

the meantime, *"if, without in any way disturbing a system, we can predict with certainty (i.e., with probability equal to unity) the value of a physical quantity, then there exists an element of physical reality corresponding to this physical quantity."*. According to these quotes, two non commuting observables can not be *real* simultaneously, even though with this thought experiment it seems like both could be known if, for example, the experiment were done twice, knowing the starting wave function was the same in the two cases.
This suggests that quantum mechanics is not complete, and it may seem necessary to search for another physical theory. For such a theory to be made, quantum mechanics should be supplemented by additional, perhaps inaccessible, variables.

1.2 The "CHSH" inequality

Despite the elegance of the EPR argument, a new physical theory would have to yield the same predictions as the quantum mechanical ones if they proved to be right. In 1964 a paper by John Bell proved that no local-realistic theory can give the same results as quantum mechanics in a situation as the one described by EPR. Our experiment is designed following the argument given by Bell [2].

1.2.1 Polarization operators

The interesting degree of freedom of this experiment is the polarization of photons. If eigenstates relative to two perpendicular polarizations along the directions making angles θ and $\theta^\perp$ with the horizontal of a coordinate system are denoted respectively as $|\theta\rangle$ and $|\theta^\perp\rangle$, the operators

$$\Sigma_1 = |\theta\rangle\langle\theta^\perp| + |\theta^\perp\rangle\langle\theta|, \tag{1.4}$$
$$\Sigma_2 = -i(|\theta\rangle\langle\theta^\perp| - |\theta^\perp\rangle\langle\theta|), \tag{1.5}$$
$$\Sigma_3 = |\theta\rangle\langle\theta| - |\theta^\perp\rangle\langle\theta^\perp|, \tag{1.6}$$

can be constructed [3]. These operators satisfy the algebra of angular momenta

$$[\Sigma_i, \Sigma_j] = 2i\varepsilon_{ijk}\Sigma_k. \tag{1.7}$$

As these operators do not commute, the Heisemberg uncertainty principle comes into play, making polarization a good candidate for the experimental proof that the EPR situation is indeed achievable.

From now on, if the polarization direction is horizontal compared to the coordinate reference system of the laboratory, its eigenstate will be denoted by $|H\rangle$, whereas if it is vertical, it will be denoted by $|V\rangle$. It is useful to note that the eigenstates of Σ_3 represent polarization along the horizontal and vertical directions, given a coordinate system; the ones of Σ_1 represent diagonal polarizations compared to the horizontal and vertical ones; the ones of Σ_2 represent left and right handed circular polarization.

1.2.2 Locality

Two photons produced by a common source get to be spatially separated and the polariza -tion of each one can be measured in arbitrary directions by one of two distant observers, Alice and Bob. Bob and Alice can choose which direction of polarization to measure, and these directions can be denoted with x and y respectively. Once the measurements are performed, they yield outcomes a and b, which may vary even when the same choices of directions x and y are made, as they are governed by a probability distribution $p(ab|xy)$. Because the wave function of photons 1 and 2 is of the form (1.1),

$$p(ab|xy) \neq p(a|x)p(b|y), \tag{1.8}$$

meaning that the outcomes are not statistically independent from each other: they are correlated.

For a theory to be local, there needs to be a set of factors, describable with variables λ, having a joint causal influence on both outcomes explaining the correlations between a and b. If all the variables were to be taken into consideration in the theory, then one would obtain that

$$p(ab|xy,\lambda) = p(a|x,\lambda)p(b|y,\lambda). \tag{1.9}$$

The variable λ may not be constant throughout all the measurements, as it may depend on uncontrollable physical quantities. The values of λ across the experiment can then be characterized by a probability distribution $q(\lambda)$. These hypotheses yield

$$p(ab|xy) = \int_\Lambda d\lambda q(\lambda)p(a|x,\lambda)p(b|y,\lambda). \tag{1.10}$$

This decomposition represents a precise definition for locality in a Bell experiment [4].

1.2.3 The "CHSH" inequality

If there are only two choices per observer $x, y \in \{0,1\}$, the possible outcomes for the polarization measurements can only take two possible values $a, b \in \{-1,1\}$ in both choices. Let's now consider the expectation value of the product ab for given (x,y)

$$\langle a_x b_y \rangle = \sum\nolimits_{a,b} abp(ab|xy) \tag{1.11}$$

and the expression

$$S = \langle a_0 b_0 \rangle + \langle a_0 b_1 \rangle + \langle a_1 b_0 \rangle - \langle a_1 b_1 \rangle. \tag{1.12}$$

If the probabilities satisfy (1.10), by rewriting (1.11), $\langle a_x b_y \rangle = \int d\lambda q(\lambda) \langle a_x \rangle_\lambda \langle b_y \rangle_\lambda$, where $\langle a_x \rangle_\lambda, \langle b_y \rangle_\lambda \in [-1,1]$ and

$$\langle a_x \rangle_\lambda = \sum\nolimits_a ap(a|x,\lambda), \tag{1.13}$$

$$\langle b_y \rangle_\lambda = \sum\nolimits_b bp(b|y,\lambda). \tag{1.14}$$

By using this expression in (1.12), one gets

$$S = \int d\lambda q(\lambda) S_\lambda, \tag{1.15}$$

where $S_\lambda = \langle a_0\rangle_\lambda\langle b_0\rangle_\lambda + \langle a_0\rangle_\lambda\langle b_1\rangle_\lambda + \langle a_1\rangle_\lambda\langle b_0\rangle_\lambda - \langle a_1\rangle_\lambda\langle b_1\rangle_\lambda$. Since $\langle a_0\rangle_\lambda, \langle a_1\rangle_\lambda \in [-1,1]$, $S_\lambda \leqslant |\langle b_0\rangle_\lambda + \langle b_1\rangle_\lambda| + |\langle b_0\rangle_\lambda - \langle b_1\rangle_\lambda|$. It is then clear that, $|S_\lambda| = 2|\langle b_{0,1}\rangle_\lambda| \leqslant 2$ and thus

$$|S| = |\langle a_0 b_0\rangle + \langle a_0 b_1\rangle + \langle a_1 b_0\rangle - \langle a_1 b_1\rangle| = \left|\int d\lambda q(\lambda) S_\lambda\right| \leqslant 2, \tag{1.16}$$

which is known as the *Clauser-Horne-Shimony-Holt* (CHSH) *inequality* [4].

1.2.4 Violation of the "CHSH" inequality

If the two photons' wave function is

$$|\Psi^+\rangle = \frac{1}{\sqrt{2}}(|H\rangle_1 \otimes |V\rangle_2 + |V\rangle_1 \otimes |H\rangle_2), \tag{1.17}$$

where $|H\rangle$ and $|V\rangle$ are eigenstates of the operator Σ_3 corresponding to polarization along the unit vectors that will be labeled as $\hat{e_1}$ and $\hat{e_2}$, with eigenvalues 1 and -1 respectively: naming x and y the directions of measurement of polarization, then according to quantum theory, if the two settings of $x \in \{0,1\}$ correspond to measurements in the directions $\hat{e}_1$ and $\frac{\hat{e}_1+\hat{e}_2}{\sqrt{2}}$ corresponding to the operators Σ_3 and Σ_1 with $|\theta\rangle = |H\rangle$ respectively, and the two settings for $y \in \{0,1\}$ are in the directions $(\cos\frac{\pi}{8}\hat{e}_1 + \sin\frac{\pi}{8}\hat{e}_2)$ and $(\cos\frac{\pi}{8}\hat{e}_1 - \sin\frac{\pi}{8}\hat{e}_2)$, then $\langle a_0 b_0\rangle = \langle a_0 b_1\rangle = \langle a_1 b_0\rangle = -\langle a_1 b_1\rangle = -\frac{1}{\sqrt{2}}$, hence

$$|S| = 2\sqrt{2} > 2, \tag{1.18}$$

in contraddiction with the locality constraint.
The "CHSH" inequality is typically violated using any of all four of what are known as the *Bell states*, which are of the form

$$|\Psi^\pm\rangle = \frac{1}{\sqrt{2}}(|H\rangle_1 \otimes |V\rangle_2 \pm |V\rangle_1 \otimes |H\rangle_2), \tag{1.19}$$

$$|\Phi^\pm\rangle = \frac{1}{\sqrt{2}}(|H\rangle_1 \otimes |H\rangle_2 \pm |V\rangle_1 \otimes |V\rangle_2). \tag{1.20}$$

2 Beam Optics

The light beam used for this experiment is generated by a pulsed laser and is characterized by a Gaussian intensity profile. The choice of this kind of beam is due to its properties, which are discussed in this section.

2.1 The paraxial wave equation

The electric and magnetic fields of the beam of light satisfy *Maxwell's equations* in free space, in particular the wave equation obtained from them

$$\nabla^2 E - \frac{1}{c^2}\frac{\partial^2 E}{\partial t^2} = 0, \tag{2.1}$$

where c is the speed of light in a vacuum. Since in the experiment the beam is linearly polarized, we can forget about the vector nature of the field and treat it as a scalar quantity [5].
By treating our beam as monochromatic, $E(r,t) = U(r)e^{i\omega t}$, and using it in (2.1), provides a partial differential equation for its complex amplitude $U(r)$, which is the *Helmholtz equation*

$$\nabla^2 U + k^2 U = 0. \tag{2.2}$$

The laser beam is highly directional and collimated, so that one can think of a solution starting from a plane wave and modulating its complex envelop making it a slowly varying function of position, so that the complex amplitude of the wave becomes

$$U(r) = A(r)e^{-ikz}. \tag{2.3}$$

If the variation of $A(r)$ and $\frac{\partial A(r)}{\partial z}$ is slow within the distance of a wavelength $\lambda = \frac{2\pi}{k}$, the wave has an approximately plane wave nature.
For the hypothesis made, within the distance $\Delta z = \lambda$, the change ΔA must be $\Delta A \ll A$ in both their real and imaginary parts. This inequality can be translated by writing $\Delta A = \left(\frac{\partial A}{\partial z}\right)\Delta z = \left(\frac{\partial A}{\partial z}\right)\lambda$, so that $\frac{\partial A}{\partial z} \ll \frac{A}{\lambda} = \frac{Ak}{2\pi}$. Thus, the inequality is translated to

$$\frac{\partial A}{\partial z} \ll kA, \tag{2.4}$$

which shows that $\frac{\partial A}{\partial z}$ must vary slowly within the distance λ, so that $\frac{\partial^2 A}{\partial z^2} \ll k\frac{\partial A}{\partial z}$. This provides that

$$\frac{\partial^2 A}{\partial z^2} \ll k^2 U. \tag{2.5}$$

Substituting (2.3) in (2.2) and neglecting $\frac{\partial^2 A}{\partial z^2}$, leads to the *paraxial Helmholtz equation*

$$\nabla_T^2 A - 2ik\frac{\partial A}{\partial z} = 0, \tag{2.6}$$

where $\nabla_T^2 = \frac{\partial^2}{\partial x^2} + \frac{\partial^2}{\partial y^2}$ is the transverse Laplacian operator.

2.2 The Gaussian beam

A simple solution to equation (2.6) is the paraboloidal wave

$$A(r) = \frac{A_1}{z} exp\left(-ik\frac{x^2+y^2}{2z}\right), \tag{2.7}$$

where A_1 is a constant. Because of this, a shifted version of it, with $q(z) = z - \xi$ substituting z is also a solution, where ξ is a constant. If $\xi = iz_0$, an imaginary number, $A(x, y, q(z))$ is the complex envelop of a Gaussian beam.
The quantity $q(z)$ is called the *q-parameter* and z_0 is the *Rayleigh range*. It is useful to write $q(z)$ in its real and imaginary parts to obtain the expressions

$$\frac{1}{q(z)} = \frac{1}{R(z)} - i\frac{\lambda}{\pi w^2(z)}, \tag{2.8}$$

$$w(z) = w_0\sqrt{1+\left(\frac{z}{z_0}\right)}, \tag{2.9}$$

$$w_0 = \sqrt{\frac{\lambda z_0}{\pi}}, \tag{2.10}$$

$$R(z) = z\left[1+\left(\frac{z}{z_0}\right)^2\right], \tag{2.11}$$

$$U(r) = \frac{A_1}{iz_0}\frac{w_0}{w(z)} exp\left[-\frac{x^2+y^2}{w^2(z)}\right] exp\left[-ikz - ik\frac{x^2+y^2}{2R(z)} + i\Xi(z)\right], \tag{2.12}$$

$$\Xi(z) = \arctan\left(\frac{z}{z_0}\right). \tag{2.13}$$

$U(r)$ is the complex amplitude of the Gaussian beam, which is the kind of beam used in the experiment.

2.2.1 Properties of the Gaussian beam

The characterizing parts of the complex amplitude of the Gaussian beam propagating in the z direction are $w(z)$ and $R(z)$, which are measures of the beam width and wavefront radius of curvature of the beam respectively. These two functions, only varying with z, depend on the two parameters z_0 and w_0.

The optical intensity of the beam is

$$I(r) = |U(r)|^2 = \left|\frac{A_1}{iz_0}\right|^2 \left[\frac{w_0}{w(z)}\right]^2 exp\left[-2\frac{x^2+y^2}{w^2(z)}\right]. \tag{2.14}$$

From now on $\left|\frac{A_1}{iz_0}\right|^2$ will be denoted as I_0. The total power of the beam can be calculated

by integrating its intensity on a transverse plane at any position z, obtaining

$$P = \frac{1}{2} I_0(\pi w_0^2), \tag{2.15}$$

which makes the meaning of w_0 very clear: it is the beam radius. In fact, the ratio of power carried within a circle of radius ρ_0 in the transverse plane to the total power at position z is

$$\frac{1}{P} \int_0^{\rho_0} I(\rho, z) 2\pi\rho d\rho = 1 - exp\left[-\frac{2\rho_0^2}{w^2(z)}\right], \tag{2.16}$$

so that the power within a circle of radius $\rho_0 = w(z)$ is $\approx 86\%$ of the total power. It is clear that $w(z)$ is the radius of the Gaussian beam, getting its lowest value at w_0, which is called the *waist radius*. The waist diameter $2w_0$ is called *spot size*.

The distance within which $|w(z)| < \sqrt{2}w_0$ is called the *depth of focus*, and it is twice the Rayleigh range so, using equation (2.10),

$$2z_0 = \frac{2\pi w_0^2}{\lambda}. \tag{2.17}$$

The wavefronts of the beam are given by

$$kz - \Xi(z) + \frac{k(x^2 + y^2)}{2R(z)} = 2\pi q \qquad q \in \mathbb{N}. \tag{2.18}$$

Their shape depends mainly on the function $R(z)$, which diverges as z goes to 0, so that the wave may be very well approximated to a plane wave when it is in its depth of focus.

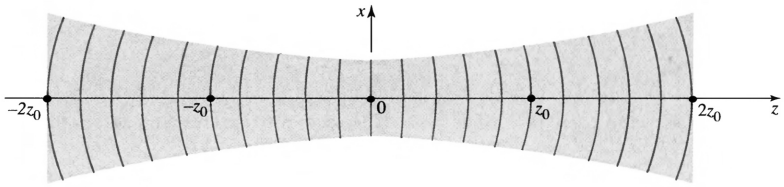

Figure 1: Wavefronts of a Gaussian beam. Figure taken from [5]

Another peculiarity of the Gaussian beam is that it remains Gaussian after the trans -mission through a thin spherical lens or the reflection from a spherical or planar mirror. This last property in particular makes such a beam sustainable in a resonator, such as the cavity of a laser.

3 The Mira-Verdi Laser

A laser is a source of intense, highly directional and coherent electromagnetic radiation. In the experiment presented in the following chapters, we will use the mode-locked Mira laser, hence this chapter presents an introduction to its functioning.

3.1 Einstein coefficients

Radiation in a solid is emitted when atoms, or molecules or electrons make a transition to a state of lower energy [6]. A transition from the quantum state of energy E_2 to the one of energy E_1 is accompanied by the emission of a photon of frequency ν, such that

$$h\nu = |E_2 - E_1|. \tag{3.1}$$

Conversely, an atom can absorb a photon of the same frequency to gain energy and leap from the state E_1 to the state E_2. These two phenomena are respectevly known as *spontaneous emission* and *absorption*.

If an atom in the state E_2 is in the presence of an electromagnetic wave of frequency ν satisfiyng equation (3.1), a photon might collide with the atom, forcing its transition to the state E_1. Through this process, called *stimulated emission*, from one photon of frequency ν, another with the same frequency and phase can be obtained.
The probability per unit time for each of the processes described are:

$$\begin{array}{cc} A & \text{probability/unit time for spontaneous emission} \\ W_{12} = B_{12}\left(\frac{du(\omega)}{d\omega}\right) & \text{probability/unit time for absorption} \\ W_{21} = B_{21}\left(\frac{du(\omega)}{d\omega}\right) & \text{probability/unit time for stimulated emission} \end{array}$$

where $\frac{du(\omega)}{d\omega}$ is the energy density per unit frequency of the incident electromagnetic radiation; A, B_{12} and B_{21} are the Einstein coefficients and $\omega = 2\pi\nu$.

It was Einstein who showed that stimulated emission must take place in order to ensure the equilibrium between an assembly of atoms and the electromagnetic field. Einstein's result also proved that in order to obtain thermal equilibrium with the radiation,

$$W_{12}N_1 = AN_2 + W_{21}N_2, \tag{3.2}$$

where N_1 and N_2 are the numbers of atoms in the quantum states of energies 2 and 1 respectively and that and the only way for (3.2) to be consistant for all temperatures is if

$$g_1 B_{12} = g_2 B_{21}, \tag{3.3}$$

$$A = \frac{\hbar\omega^3}{\pi^2 c^3} B_{21}. \tag{3.4}$$

3.1.1 Lineshape broadening

The radiation emitted in atomic transitions is not perfectly monochromatic and its shape is described by the *spectral lineshape function*, which peaks at the frequency satisfying equation (3.1) [7]. Only phenomena of lineshape broadening concering solids will be considered, as the Mira is a solid state laser.

Atoms in excited states drop to lower levels at a rate $\tau = \frac{1}{A}$, where A is the Einstein coefficient. In accordance with the energy-time uncertainty principle

$$\Delta E \Delta t \geq \frac{\hbar}{2}, \tag{3.5}$$

setting $\Delta E = \hbar \Delta\omega$ and $\Delta t = \tau$,

$$\Delta\omega \geq \frac{1}{2\tau}. \tag{3.6}$$

This uncertainty on the frequency produces the so called *lifetime broadening* of the spectral line.
In solids, and in particular in the Mira, atoms may de-excite from the upper level to the lower one by emitting phonons instead of photons. Because of this, one can write the rate of change of atoms in level two as

$$\frac{dN_2}{dt} = -AN_2 - \frac{N_2}{\tau_{NR}} = -\left(\frac{1}{\tau} + \frac{1}{\tau_{NR}}\right) N_2, \tag{3.7}$$

where τ_{NR} is the non-radiative relaxation time. Non radiative transitions shorten the lifetime of the excited state so that

$$\frac{1}{\tau_{eff}} = \left(\frac{1}{\tau} + \frac{1}{\tau_{NR}}\right), \tag{3.8}$$

where τ_{eff} is the actual lifetime of the excited state, which will take the place of τ in equation (3.6).

3.2 The laser

The acronym laser stands for "Light Amplification by Stimulated Emission of Radiation". As suggested by the name, its proper functioning relies on the production of a great amount of photons by stimulated emission. If an assembly of atoms with density N_t $atoms/cm^3$, is such that

$$N_t = N_1 + N_2, \tag{3.9}$$

where N_1 and N_2 are the densities of atoms in states 1 and 2, and radiation of frequency ω satisfying (3.1) is incident on the assembly, the rate of change of the photon density N_γ will be

$$\frac{dN_\gamma}{dt} = AN_2 - W_{12}N_1 + W_{21}N_2, \tag{3.10}$$

where, to obtain a coherent beam of light, we want $W_{21}N_2 >> AN_2$, so that

$$\frac{dN_\gamma}{dt} \approx B\left(\frac{du(\omega)}{d\omega}\right)(N_2 - \frac{g_2}{g_1}N_1). \tag{3.11}$$

In this situation the density of photons will increase only if $N_2 > \frac{g_2}{g_1}N_1$, but this condition is not satisfied in thermal equilibrium, as according to Boltzmann statistics $\frac{N_2}{N_1} = \frac{g_2}{g_1}e^{-\hbar\omega} < \frac{g_2}{g_1}$ [6]. The only possibility of obtaining a gain in photons is to create what is called a *population inversion* in the assembly of atoms.

A situation of a 2 level laser, where equation (3.9) is satisfied, is in fact not realistic for the presence of population inversion. The Mira is a *four level laser*, meaning four energy states are used to ensure a stable population inversion. Atoms are pumped from the ground state to level 3 from where they decay rapidly to level 2, thus creating population inversion with respect to level 1. The decay rate from level 1 back to the ground state is fast to prevent atoms accumulating in that level, ensuring that $N_2 > \frac{g_2}{g_1}N_1$. The pumping process from the ground state to level 3 is achieved with the use of the Verdi laser, in our case.

The laser tipically consists of a resonating cavity in which there is a gain medium. Each time light bounces in the cavity going through the gain medium, stimulated emission occurs. The output emerges from an optical component of the resonator, which has partially transmitting coating.

3.2.1 Laser modes

The cavity of the laser serves as a resonator, which has a great effect on the properties of the beam. The modes of electromagnetic radiation generated by the laser are the Hermite Gaussian beams [7]. These modes can be studied independently in their so called *longitudial* and *transverse* modes, meaning respectively the factor depending on the direction of propagation z and the one depending on the other two coordinates (x, y). The beam in the cavity must be a standing wave with nodes at the mirrors because of their high reflectivity. Hence, the wave must satisfy the condition

$$L_{cav} = q\frac{\lambda}{2} = q\frac{\pi c}{n_{cav}L_{cav}} \tag{3.12}$$

where q is a natural number, L_{cav} is the length of the cavity and n_{cav} is the refractive index of the medium. This implies that the longitudinal modes are separated in frequency by the difference

$$\nu_F = \frac{c}{2n_{cav}L_{cav}} \tag{3.13}$$

and can be defined by an integer q, a factor such that $\nu_{mode} = \nu_0 + q\nu_F$, where ν_0 satisfies equation (3.1).

It is normal to operate the laser on the transverse Gaussian mode, for its already discussed properties. Different transverse modes have different spatial distributions,

so that an aperture of controllable shape placed inside the resonator can be used to attenuate undesired modes. The mirrors can be designed to favor a particular one, too [5]. Longitudinal modes can also be chosen: to remove light produced by unwanted transitions in the gain medium whose populations are inverted by the pumping mechanism, a prism can be put inside the cavity to deviate the light from the resonator.

3.2.2 Mode locking

A laser can oscillate on many longitudinal modes, with frequencies separated according to equation (3.13). External means can be used to couple them and *lock* their phases together. The modes can then be regarded as the components of a Fourier series expansion of a periodic function of time of period $T_F = \frac{1}{\nu_F}$, which constitute a pulse train [5].

We will approximate every laser mode by a uniform plane wave propagating in the z direction with a velocity $\frac{c}{n_{cav}}$. The total complex wave function may be written as

$$U(z,t) = \sum_q A_q exp\left[2\pi i\nu_q\left(t - \frac{zn_{cav}}{c}\right)\right], \tag{3.14}$$

$$\nu_q = \nu_0 + q\nu_F \qquad q \in \mathbb{Z}, \tag{3.15}$$

where A_q is the complex envelop of the mode and ν_0 is the frequency satisfying condition (3.1). Since the modes interact with different groups of atoms in an inhomogeneously broadened medium, their phases $arg\{A_q\}$ are random and statistically independent. Substituting (3.15) in (3.14) provides

$$U(z,t) = \mathsf{A}\left(t - \frac{zn}{c}\right) exp\left[2\pi i\nu_0\left(t - \frac{zn}{c}\right)\right], \tag{3.16}$$

$$\mathsf{A(t)} = \sum_q A_q exp\left[\frac{2\pi iqt}{T_F}\right]. \tag{3.17}$$

Since $\mathsf{A(t)}$ is a periodic function of the period T_F, and thus $A(t - \frac{zn}{c})$ is periodic of period $\frac{1}{n_{cav}}T_F = 2\frac{L_{cav}}{c}$, if the magnitudes and phases of the complex coefficients A_q are properly chosen, $\mathsf{A(t)}$ may be made to take the form of periodic narrow pulses.
Let's assume we have M modes ($q = 0, \pm1, ..., \pm S$, so that $M = 2S + 1$) whose complex coefficients are all equal to A. Then

$$\mathsf{A(t)} = A\sum_{-S}^{S} exp\left(\frac{2\pi iqt}{T_F}\right) = A\frac{x^{S+1} - x^{-S}}{x - 1} = A\frac{x^{S+\frac{1}{2}} - x^{-S-\frac{1}{2}}}{x^{\frac{1}{2}} - x^{-\frac{1}{2}}}, \tag{3.18}$$

which can also be written as

$$\mathsf{A(t)} = A\frac{\sin\left(\frac{M\pi t}{T_F}\right)}{\sin\left(\frac{\pi t}{T_F}\right)}, \tag{3.19}$$

so that the intensity of the pulse is

$$I(t,z) = |A|^2 \frac{\sin^2\left[\frac{M\pi(t-\frac{zn_{cav}}{c})}{T_F}\right]}{\sin^2\left[\frac{\pi(t-\frac{zn_{cav}}{c})}{T_F}\right]}. \tag{3.20}$$

The shape of the mode-locked pulse is therefore dependent on the number of modes M, which is proportional to the atomic linewidth $\Delta\nu$. The pulse duration τ_{pulse} is inversely proportional to the linewidth, which, as illustrated in fig. 2, is a periodic function of time of period $T_F = \frac{2n_{cav}L_{cav}}{c}$.

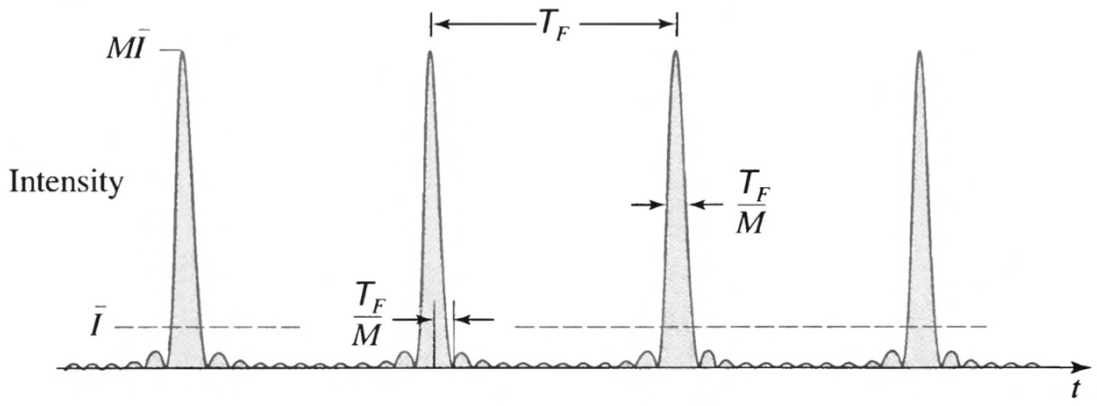

Figure 2: Intensity of the periodic pulse train resulting from the sum of M laser modes of equal magnitudes and phases. The full width at half maximum of the pulse is M times smaller than T_F, and is considered as the duration of the pulse. Figure taken from [5].

3.2.3 The Mira laser

The Mira laser is a solid state laser, whose gain medium is titanium doped sapphire. This kind of medium is tunable over a substantial range of wavelengths. In this experiment the Mira is mode-locked, to provide extremely short pulses of duration $\delta t \approx 150$ fs with a period $T_F = 13$ ns. The material is mostly sapphire, so its refractive index is $n_{cav} \approx 1,76$. The system behaves well as a four level laser, whose energy levels are shown in fig. 4 (a). The laser transition from state 2 to state 1 in fig. 4 can be tuned over a few tens of nm by making use of a rotatable birefringent filter installed at Brewster's angle within the cavity, which acts as a bandpass filter for the polarized intercavity beam. Greater changes in wavelength can be achieved by adjusting the internal optics, a prism in particular, since the cavity group velocity dispersion changes with wavelength. Wavelengths in the range of 700 nm up to 1050 nm can be accessed, even though it is used at $\lambda = 808$ nm in this experiment.

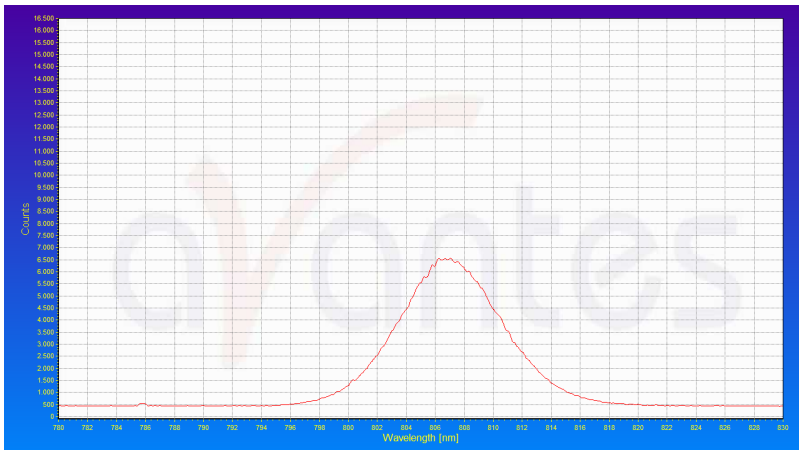

Figure 3: The spectral lineshape function of the Mira's beam (not normalized). The shape of the spectrum mainly depends on mode locking.

In fig. 4 (b) a sketch of the internal optics of the laser is shown. A polarizer is also placed inside the cavity, as it is fundamental for this experiment for the light beam to be linearly polarized. The pump is the Verdi laser, a single mode continuous laser at $\lambda = 532$ nm, pumping at $P = 17,50$ W.

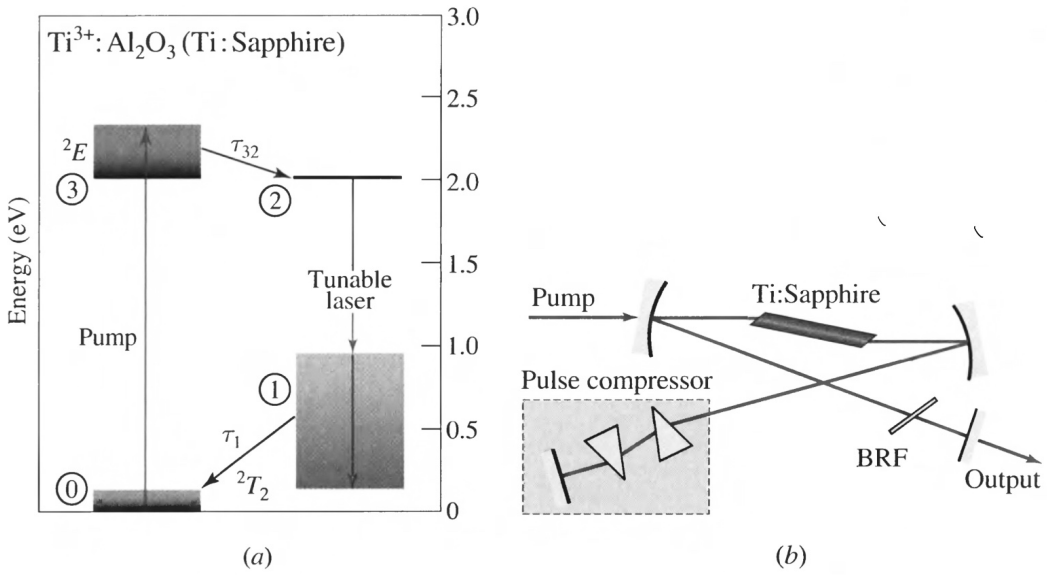

Figure 4: (a) selected energy bands of $Ti^{3+} : Al_2O_3$. The arrow going from state 2 to state 1 indicates the principal laser transition of this system, which is tunable between 700 nm and 1050 nm. Shading in the bands indicates a decrease in relative occupancy. (b) Sketch of the internal optics of the Mira laser. Figure taken from [5].

4 Non-linear Optics

Many optical phenomena are exploited in this experiment, including two which let the creation of polarization entangled photons at the optimal frequency for the photon detectors to work: the second harmonic generation (SHG) and the spontaneous parametric down conversion (SPDC).

4.1 The nonlinear wave equation

A nonlinear dielectric medium is defined as one in which the relation between the polarization density vector P and the electric field vector E is not linear. For homogeneous and isotropic media, $D = \varepsilon E$, where $D = \varepsilon_0 E + P$ is the *electric displacement*, so that $\nabla \cdot E = 0$. This way,

$$\nabla^2 E - \frac{1}{c^2}\frac{\partial^2 E}{dt^2} = \mu_0 \frac{\partial^2 P}{\partial t^2}. \tag{4.1}$$

If P is nonlinear, nondispersive and nonmagnetic, $P = \Psi(E(r,t))$. If the medium is actually isotropic, $E \parallel P$, so that each component of P, P_i with $i = 1, 2, 3$, can be written as a Taylor expansion in a polinomial in E_i, whose coefficients are not known. Since in our case the beam is linearly polarized, we can treat P as a scalar quantity. By convention [5] we will write the expansion of P as

$$P = \varepsilon_0 \chi E + P_{NL}, \tag{4.2}$$

$$P_{NL} = 2\chi^{(2)} E^2 + 4\chi^{(3)} E^3 + \cdots, \tag{4.3}$$

which makes it possible to write (4.1) as

$$\nabla^2 E - \frac{1}{c^2}\frac{\partial^2 E}{dt^2} = -\delta, \tag{4.4}$$

$$\delta = -\mu_0 \frac{\partial^2 P_{NL}}{\partial t^2}. \tag{4.5}$$

4.1.1 Second harmonic generation

As the coefficients of the expansion of P decrease rapidly with the increasing orders of E, it is practical to consider only the linear and quadratic terms of its expression. This way, if $E = Re\{U(\omega)exp(i\omega t)\}$, $P_{NL} = 2\chi^{(2)}E^2$, so that

$$P_{NL}(t) = P_{NL}(0) + Re\{P_{NL}(2\omega)exp(2i\omega t)\}, \tag{4.6}$$

$$P_{NL}(0) = \chi^{(2)} U(\omega) U^*(\omega), \tag{4.7}$$

$$P_{NL}(2\omega) = \chi^{(2)} U^2(\omega). \tag{4.8}$$

By substituting (4.6) in (4.4), one sees that the source of the electric field due to the polarization vector, δ, has a component at frequency 2ω with complex amplitude

$s(2\omega) = 4\mu_0\omega^2\chi^{(2)}U^2(\omega)$ which radiates an optical field at frequency 2ω.
The emissions are added coherently so that the intensity of the second harmonic wave is proportional to the square of the length of the interaction volume L. It is useful to define the *efficiency of second harmonic generation*

$$\eta_{SHG} = \frac{I(2\omega)}{I(\omega)} = C^2\frac{L^2}{A^2}P, \tag{4.9}$$

since $I(\omega) = \frac{P}{A}$ where A can be considered as the area of the circle of radius w_0 of the Gaussian beam, since it is focused by a lens on the nonlinear crystal to optimize η_{SHG}. C is a constant dependent on ω^2 and $\chi^{(2)2}$ [5]. The pulsed nature of the beam also manages to optimize η_{SHG}, since the energy is confined in time and reaches high peaked powers.

4.2 Three wave mixing

If a wave with two different harmonic components at frequencies ω_1 and ω_2 goes through a nonlinear crystal, P_{NL} will contain five frequencies: 0, $2\omega_1$, $2\omega_2$, $\omega_1+\omega_2$ and $\omega_1-\omega_2$. Not all of these waves necessarily generate, as the conditions of *phase matching* and *frequency matching* have to be satisfied.
This process can be explained from a photon-optics perspective as an interaction between three photons: two photons of low frequency annihilate to create a photon of higher frequency. This process can happen in reverse, too, with one photon of high frequency annihilating to create two of lower energy. This is the process exploited to create entangled states from a common source. Still, frequency and phase matching have to be satisfied for the process to happen.

4.2.1 Frequency and phase matching

In the process of three wave mixing, both energy and momentum have to be conserved, so that the following relations have to be satisfied by the three photons involved:

$$\hbar\omega_1 = \hbar\omega_2 + \hbar\omega_3, \tag{4.10}$$
$$\hbar k_1 = \hbar k_2 + \hbar k_3, \tag{4.11}$$

where the subscripts $1, 2, 3$ stand for the high energy photon an the lower energy photons respectively; k_1, k_2 and k_3 are the wave vectors of the three photons. These two equations are referred to as *frequency* and *phase matching conditions*.

Since the three photons do not necessarily have parallel wave vectors, the phase matching condition can be translated to

$$\omega_1 n_1 \hat{u}_1 = \omega_2 n_2 \hat{u}_2 + \omega_3 n_3 \hat{u}_3, \tag{4.12}$$

where $\hat{u}_1$, $\hat{u}_2$ and $\hat{u}_3$ are the unit vectors in the directions of the wave vectors and n_1, n_2 and n_3 are the refractive indexes of the crystal, depending on the polarization and

direction of the photon in the medium [5]. Equation (4.12) can be written as three scalar equations in spherical coordinates, denoting with α_2 and α_3 the polar angles of the two photons and with β_2 and β_3 the azimuthal, and placing the x direction along the wave vector of the pump

$$\begin{aligned} \omega_2 n_2 \cos\alpha_2 \sin\beta_2 + \omega_3 n_3 \cos\alpha_3 \sin\beta_3 &= \omega_1 n_1, & (4.13)\\ \omega_2 n_2 \sin\alpha_2 \sin\beta_2 + \omega_3 n_3 \sin\alpha_3 \sin\beta_3 &= 0, & (4.14)\\ \omega_2 n_2 \cos\beta_2 + \omega_3 n_3 \cos\beta_3 &= 0. & (4.15) \end{aligned}$$

This way, adding the *degenerate condition* $\omega_2 = \omega_3$ one has three equations of four variables α_1, α_2, β_1 and β_2 to know where the degenerate photons are.

4.2.2 Spontaneous parametric down conversion

In the experiment, a BBO ($\beta - BaB_2O_4$) crystal is used to obtain SPDC. When the intense linearly polarized pump laser beam shines it, pairs of photons referred as *idler (i)* and *signal (s)* are probabilistically generated from the crystal simultaneously. The probability is maximized when the conditions (4.10) and (4.11) are satisfied. The photons produced have orthogonal polarizations, named *extraordinary (e)* and *ordinary (o)*. The process is thus called *SPDC type II*: from a photon of polarization (e), two of polarizations (e) and (o) are obtained. With type II phase-matching, the two photons are emitted over two different cones if they are degenerate, (i.e. $\omega_i = \omega_s = \frac{1}{2}\omega_1$) because of birefringence effects and equations (4.13), (4.14) and (4.15). The relative position of the two cones depends on the angle between the laser beam and the optical axis of the crystal: in the collinear situation the two cones are tangent; if the angle between the pump and the crystal's optical axis is decreased they separate and if it is increased the cones intersect, as shown in fig. 5 [8].

The polarizations (o) and (e) can of course be chosen to be $|H\rangle$ and $|V\rangle$. The photons produced in the intersections of the cones are in a superposition of states, since it is not possible to know which one of the pair is in the state $|H\rangle$ or $|V\rangle$ without making a polarization measurement. The state of the created photons is thus of the form (1.1) and it can be written as (1.17), aside from the phase shift due to the birefringent properties of the crystal.

More precisely [9], a SPDC two photon state can be expressed as

$$N \int d^2k_s d^2k_i d\omega_s d\omega_i A_p(k_s + k_i, \omega_s + \omega_i) sinc\left(\frac{\Delta k_z L}{2}\right) |k_s, \omega_s\rangle \, |k_i, \omega_i\rangle \,, \qquad (4.16)$$

where k_i and k_s are the transverse momentum coordinates of the idler and signal photons; $|k, \omega\rangle = a^\dagger(k, \omega)\,|0\rangle$ ($a^\dagger$ is the creation operator and $|0\rangle$ is the vacuum state of the photon); $A_p(k, \omega)$is the pump profile in the momentum-frequency space; N is the normalization constant and L is the length of the crystal;

$$\Delta k_z = k_{pz}(k_i + k_s, \omega_i + \omega_s) - k_{sz}(k_s, \omega_s) - k_{iz}(k_i, \omega_i)$$

is the *longitudinal phase mismatch*, where $k_z(k,\omega) = \sqrt{\left[\frac{n(\omega)\omega}{c}\right]^2 - k^2}$. The pump wave function is usually chosen to be Gaussian.
The phase matching condition is satisfied when $\Delta k_z = 0$. In type II phase matching, if this condition is satisfied and the two photons are degenerate, k_i and k_s lie in cones such as the ones shown in fig. 5.

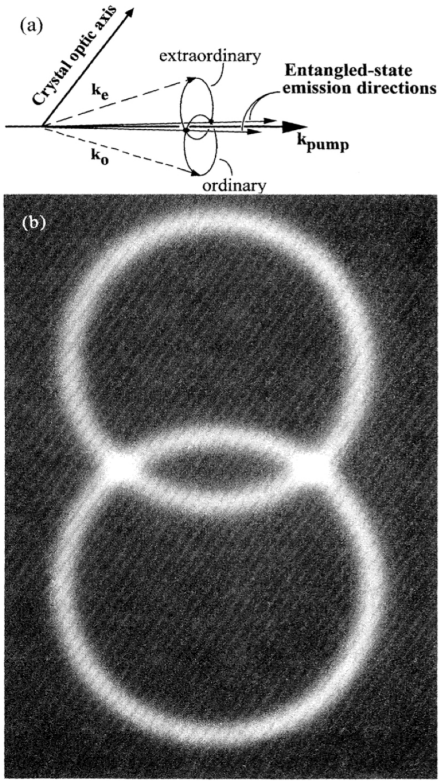

Figure 5: (a) Type II phase matching. Correlated photons lie on opposite sides of the pump beam. (b) Down conversion photons. Figure taken from [8].

4.2.3 The wave function after SPDC

The actual wavefunction of the two photons in the intersections of the cones is

$$|\psi\rangle = \frac{1}{\sqrt{2}}(|H\rangle_1 \otimes |V\rangle_2 + e^{i\alpha} |V\rangle_1 \otimes |H\rangle_2), \tag{4.17}$$

since a phase shift α occurs because of the birefringence of the crystal [8], making the extraordinary and ordinary photons run in different directions and with different velocities u_e and u_o inside the crystal. Despite that, they become collinear outside the crystal. The longitudinal and transverse walk-offs are maximal for pairs created near the entrance face

of the crystal, since they are proportional to the length of the path run across. Therefore, a time delay

$$\delta t = L\left(\frac{1}{u_o} - \frac{1}{u_e}\right), \tag{4.18}$$

where L is the length of the crystal, occurs. The lateral displacement is

$$d = L\tan\phi, \tag{4.19}$$

where ϕ is the angle between the two photons' directions inside the crystal.

If $\delta t > \tau_c$, the coherence time of the down conversion light, the photons become distinguishable by the time of observation of the single photon, inevitably changing their wavefunction taking away the polarization superposition, making the state separable. Also, if d is greater than the coherence width, the photons can be labeled by their spacial location therefore creating the same situation. Because of this, the dimensions of the crystal are carefully chosen and some expedients are used to compensate the walk-off effects. Since the wavefunction is more complicated than the Bell states in (1.19), some expedients are used to change α during the path of the photons in the experimental setup, too.

To compensate the longitudinal walk-off, two other BBO crystals are placed in the experimental setup: one in each path for the two photons. The two crystals are half as long as the first one to compensate for both of them. The optical axis of the two crystals are rotated of $\frac{\pi}{2}$ in comparison with the one of the first one, so that the time delays of the two photons compensate perfectly making $\delta t = 0$.

To create the phase shift of α to 0 or π and compensate the walk-off effects, the use of birefringent devices like qarter wave plates, whose properties are discussed in the next section, is therefore necessary. With the experimental setup used, described in section 6, both of the Bell states in (1.19) can be created to violate the CHSH inequality.

5 Polarization Optics

Many birefringent devices are placed within the experimental setup. In this section, the formalism of polarization optics and the role of birefringent devices in the experiment will be discussed.

5.1 The Jones vectors

The property of polarization of light depends on the relative amplitude and phase of the electric field along the x and y directions. From a photon optics perspective, polarization is determined by the probability amplitudes of a photon to be transmitted by a polarizer in two orthogonal directions. The Jones vectors incorporate all the information about the polarization of an optical field or a photon in a two dimensional vector. If the complex amplitude of an electric field is $E = E_x\hat{u}_x + E_y\hat{u}_y$, the corresponding Jones vector is

$$\frac{1}{|E|}\begin{pmatrix}E_x\\E_y\end{pmatrix} = \frac{1}{|E|}\begin{pmatrix}|E_x|e^{i\phi_x}\\|E_y|e^{i\phi_y}\end{pmatrix}, \tag{5.1}$$

where $\phi_{x,y}$ is the phase of $E_{x,y}$. The overall phase of the vector does not change its nature, so that two Jones vectors differing in their overall phase are considered to be equivalent. In the quantum mechanical case, it is possible to associate a single horizontally polarized photon to a vector in a 2-dimensional Hilbert space, equivalent to the one in which the Jones vectors are present [10]. The only difference is that while in the classical case the entries of the vectors are proportional to the electric field, in the case of the single photon they are the probability amplitudes for the photon to pass through a polarizer. A general state of a photon can be written as $|\psi\rangle = \alpha\,|H\rangle + \beta\,|V\rangle$ where $|\alpha|^2 + |\beta|^2 = 1$. A photon in such a state, neglecting all of its other degrees of freedom, is named *qubit*, and belongs to a 2-dimensional complex Hilbert space, so that it is possible to write $|\psi\rangle \in \mathbb{C}^2$. It is common to write

$$|H\rangle = \begin{pmatrix}1\\0\end{pmatrix}, \tag{5.2}$$

$$|V\rangle = \begin{pmatrix}0\\1\end{pmatrix}, \tag{5.3}$$

$$|+\rangle = \frac{1}{\sqrt{2}}\begin{pmatrix}1\\1\end{pmatrix} = \frac{1}{\sqrt{2}}(|H\rangle + |V\rangle), \tag{5.4}$$

$$|-\rangle = \frac{1}{\sqrt{2}}\begin{pmatrix}1\\-1\end{pmatrix} = \frac{1}{\sqrt{2}}(|H\rangle - |V\rangle), \tag{5.5}$$

where $|H\rangle$ and $|V\rangle$ are the eigenstates of the operator Σ_3 and $|+\rangle$ and $|-\rangle$ are eigenstates of operator Σ_1 defined in (1.6) and (1.4), given $|\theta\rangle = |H\rangle$. The eigenstates of operator Σ_2 are given by $|R\rangle = \frac{1}{\sqrt{2}}(|H\rangle + i\,|V\rangle)$ and $|L\rangle = \frac{1}{\sqrt{2}}(|H\rangle - i\,|V\rangle)$ which correspond to right and left circularly polarized light. In this basis, the polarization operators correspond to the Pauli matrices, which also describe the spin operators.

5.2 Linear polarizers

A linear polarizer is a device that transmits only the photons whose polarization lies along the direction of its transmission axis and reflects the photons with orthogonal polarization. Therefore, a photon whose wave function can be represented by a Jones vector $\frac{1}{\sqrt{2}}(\sqrt{p_1}\,|\theta\rangle + \sqrt{p_2}\,|\theta^{\perp}\rangle)$ encountering a linear polarizer whose transmission axis is along the direction θ can be described mathematically as a projector $|\theta\rangle\langle\theta|$ or $|\theta^{\perp}\rangle\langle\theta^{\perp}|$ acting on the wave function of the photon, where the nature of the projector depends on whether or not the photon is transmitted.

Since the polarizer in the experimental setup is always left with its transmission axis lying in the direction of (o), the ordinary polarization of eigenstate $|H\rangle$, the projector associated with transmission is of the form

$$|H\rangle\langle H| = \begin{pmatrix} 1 & 0 \\ 0 & 0 \end{pmatrix}. \tag{5.6}$$

5.3 Wave plates

It is possible to change the polarization of a beam or of single photons by introducing a phase delay between the two components of the Jones vector. This is achievable through the use of wave plates, which are formed from a doubly refracting material, meaning its refractive index depends on the direction of polarization. The waveplates used have an axis of maximum index n_1 called the *slow axis* and an axis of minimum index n_2 called the *fast axis* lying orthogonal to each other.

If the wave plate has thickness d, the phase accumulated after the path will be n_1kd for light polarized along the slow axis and n_2kd for the fast axis. The relative phase shift desired is either of $\frac{\pi}{2}$ for *quarter wave plates*, $\frac{\lambda}{4}$, or of π for *half wave plates*, $\frac{\lambda}{2}$. The polarization of light polarized in the direction of the fast or slow axis will not be affected by the passage through a wave plate.

A half wave plate whose fast and slow axis are along the horizontal and vertical directions of the laboratory coordinate system can be represented with the matrix

$$S^{\frac{\lambda}{2}} = \begin{pmatrix} 1 & 0 \\ 0 & -1 \end{pmatrix} \tag{5.7}$$

acting on a Jones vector, so that its matrix when its fast axis makes an angle θ with the horizontal can be derived using a simple rotation $R(\theta) = \begin{pmatrix} \cos\theta & \sin\theta \\ -\sin\theta & \cos\theta \end{pmatrix}$:

$$S_{\theta}^{\frac{\lambda}{2}} = R(-\theta)S^{\frac{\lambda}{2}}R(\theta) = \begin{pmatrix} \cos 2\theta & \sin 2\theta \\ \sin 2\theta & -\cos 2\theta \end{pmatrix}. \tag{5.8}$$

It is worth noticing that (5.7) is the Pauli matrix corresponding to the operator Σ_3 in the $\{|H\rangle, |V\rangle\}$ basis. Similarly, for the quarter wave plate whose fast axis is horizontal

$$S^{\frac{\lambda}{4}} = \begin{pmatrix} 1 & 0 \\ 0 & -i \end{pmatrix}, \tag{5.9}$$

and if its fast axis makes an angle θ with the horizontal

$$S_{\theta}^{\frac{\lambda}{4}} = \begin{pmatrix} \cos^2\theta - i\sin\theta & (1+i)\sin\theta\cos\theta \\ (1+i)\sin\theta\cos\theta & \sin^2\theta - i\cos^2\theta \end{pmatrix}. \tag{5.10}$$

It is also important to note that if $\theta = \pm\frac{\pi}{4}$, the effect of a half wave plate on the photon polarization states $|H\rangle$ and $|V\rangle$ is

$$S_{\pm\frac{\pi}{4}}^{\frac{\lambda}{2}} |H\rangle = \pm|V\rangle, \tag{5.11}$$

$$S_{\pm\frac{\pi}{4}}^{\frac{\lambda}{2}} |V\rangle = \pm|H\rangle, \tag{5.12}$$

and that if the angle is $\pm\frac{\pi}{8}$,

$$S_{\pm\frac{\pi}{8}}^{\frac{\lambda}{2}} |H\rangle = |\pm\rangle, \tag{5.13}$$

$$S_{\pm\frac{\pi}{8}}^{\frac{\lambda}{2}} |V\rangle = \pm|\mp\rangle. \tag{5.14}$$

6 Experimental Setup and Alignment Procedure

Figure 6: The experimental setup

The experimental setup used, whose picture is shown in fig. 6, can be treated in two parts, shown in fig. 7 and fig. 8 respectively: the one before the beam shines the BBO crystal and the one after.

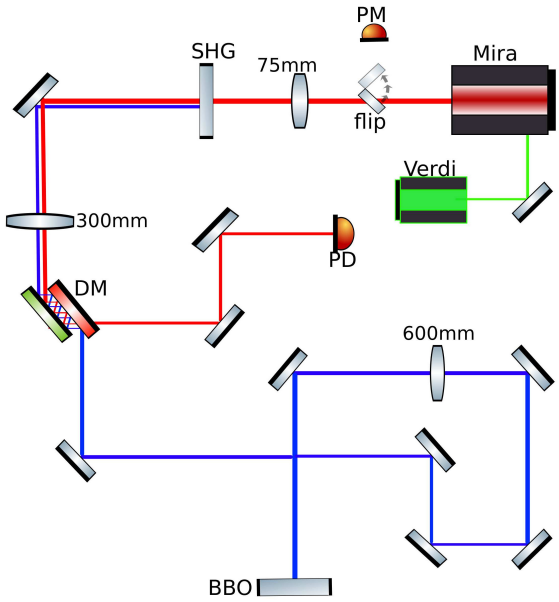

Figure 7: First part of the experimental setup. The PM, power meter, is used to check the power of the laser for optimization; SHG is the label for the crystal producing second harmonic generation; the DM is a dichroic mirror, reflecting blue light at 404 nm and transmitting the light at 808 nm to avoid noise in the detectors placed in the second part of the setup; The photodiode, PD, is used as a time trigger to have a time reference when using the data analysis programs; the BBO is the crystal responsible for SPDC.

The purpose of the first part of the experimental setup is to produce as much light at 404 nm as possible in order to shine the BBO crystal and produce the entangled photons. It is therefore necessary to optimize η_{SHG} of equation (4.9), as described in section 4.1.1. The ideal situation is achieved when the pump laser is at its maximum power and at the desired wavelength, of around 3.10 W and 808 nm and the beam is at its beam waist, of around 100 μm, at the SHG crystal. The optimizations of the power and wavelength of the laser are obtained by changing its internal optics shown in figure 4, while its focusing is guaranteed by the positioning of the lens, mounted on a micrometer stage.

After the SHG, it is necessary to separate the 808 nm beam from the 404 nm one in order to avoid red noise, to which the detectors are very sensitive. For this purpose, two dichroic mirrors are placed as shown in the figure. The two-frequency beam is reflected and transmitted four times in the system so that almost all the red light is lost and driven towards the photodiode. This is used as a time trigger, as the Mira emits a pulse of light every 13 ns. Again, it is necessary to focus the blue beam in the BBO crystal to optimize its efficiency and produce as many entangled pairs as possible.

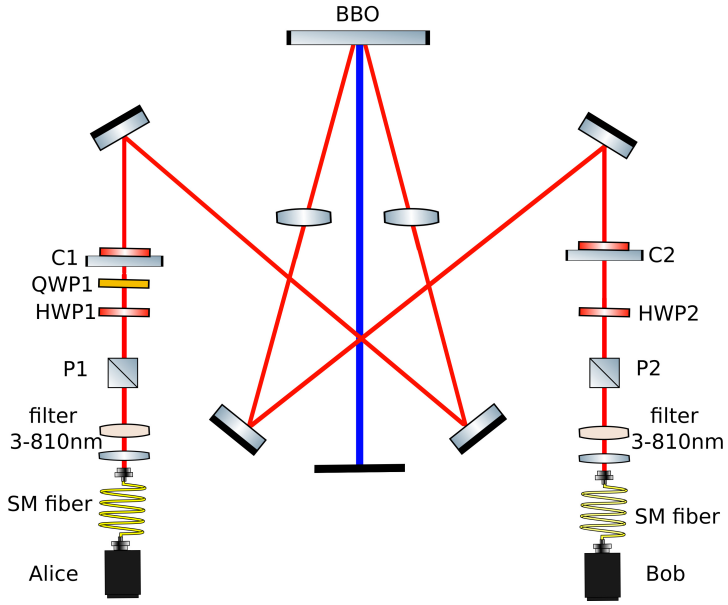

Figure 8: Second part of the experimental setup. SPDC occurs in the BBO crystal. The systems C1 and C2 are the two other BBO crystals (half the length of the first one). QWP1 is the quarter wave plate while HWP1 and HWP2 are the two half wave plates. P1 and P2 are the linear polarizers. A filter and a lens are placed before the single mode fiber in each path. Both of the fibers are connected to a SPAD, the single photon detectors named Alice and Bob.

As already discussed in section 4.2.3, the systems C1 and C2 are necessary to compensate the longitudinal walk-off effects making (4.18) zero, while the quarter wave plate is used to eliminate the phase in the state of the two photons (4.17). The two half wave plates, HWP1 and HWP2, are used to make the wave function of the photons

transform as will be discussed in section 6.1. The two linear polarizers are left still, with their transmission axis in the direction of (o), corresponding to $|H\rangle$. The two filters are used to limit the noise, especially at low wave lengths, and optimize the visibilities (see section 7.1). The two lenses placed before the single mode fibers ensure that the incident photons propagate in a direction lying in their acceptance angle. The fibers are fixed on a three axes nanometric stage, making it possible to move them slightly to get them in the optimal position of focus relative to the position of the lenses.

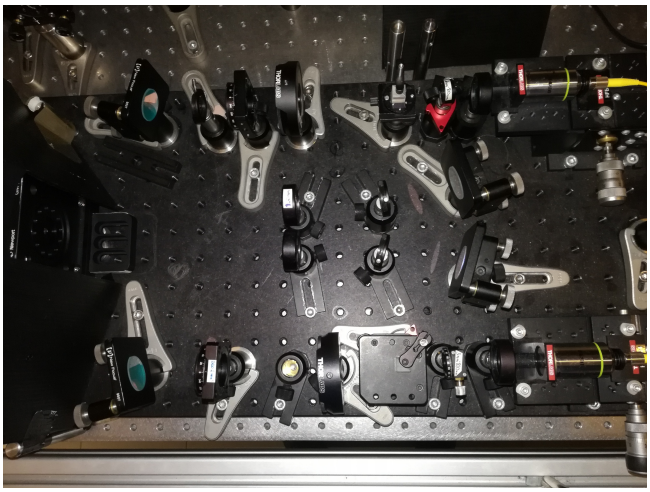

Figure 9: Second part of the experimental setup.

The detectors used are *single photon avalanche detectors* (SPAD). A photon entering a SPAD causes photoelectric effect; the electric field inside the detector causes the photo electron to ionize other atoms through collision, thereby creating an *avalanche*. These electrons cause a measurable macroscopic current, which can be detected. The SPADs used have an efficiency of $\approx 50\%$ with photons at $\lambda = 810$ nm.

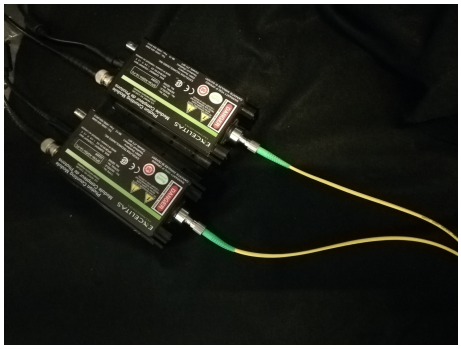

Figure 10: The SPADs used in the experiment.

6.1 Rotation of the polarizers and the QWP

A Bell state

$$|\Psi^{\pm}\rangle = \frac{1}{\sqrt{2}}(|H\rangle_1 \otimes |V\rangle_2 \pm |V\rangle_1 \otimes |H\rangle_2) \tag{6.1}$$

interacting with the two half wave plates HWP1 and HWP2 shown in fig. 8 is transformed in a state $|\Psi'^{\pm}\rangle$, depending on the angles θ of the matrix $S_{\theta}^{\frac{\lambda}{2}}$ in (5.8). The effect of the half wave plates combined with the linear polarizers P1 and P2 (whose transmission axes are fixed in the direction of $|H\rangle$) on $|\Psi^{\pm}\rangle$ corresponds to a projective measurement of polarization of the two photons in directions depending on the angles made by HWP1 and HWP2 with the horizontal.

To show this, it is possible to consider a linearly polarized photon, whose state is

$$|\varphi\rangle = \alpha\,|H\rangle + \beta\,|V\rangle\,, \tag{6.2}$$

which can always be written in terms of other Jones vectors as

$$|\varphi\rangle = (\alpha\cos\theta + \beta\sin\theta)\,|\theta\rangle + (\alpha\sin\theta - \beta\cos\theta)\,|\theta^{\perp}\rangle\,, \tag{6.3}$$

where $|\theta\rangle$ is an arbitrary Jones vector corresponding to linear polarization making an angle θ with $|H\rangle$ and $|\theta^{\perp}\rangle$ corresponds to polarization orthogonal to θ. After the passage through a polarizer with its transmission axis along the direction of $|\theta\rangle$, the probability for it to be transmitted is

$$p(\theta) = |\,\langle\theta|\varphi\rangle\,|^2 = |\alpha\cos\theta + \beta\cos\theta|^2. \tag{6.4}$$

On the other hand, if the photon described by (6.2) goes through a half wave plate rotated by an angle $\frac{\theta}{2}$ compared to the direction of $|H\rangle$,

$$|\varphi\rangle \longrightarrow |\varphi'\rangle = (\alpha\cos\theta + \beta\sin\theta)\,|H\rangle + (\alpha\sin\theta - \beta\cos\theta)\,|V\rangle\,, \tag{6.5}$$

which means that its probability to be transmitted by a polarizer whose transmission axis lies in the direction of $|H\rangle$ is

$$p(H) = |\,\langle H|\varphi'\rangle\,|^2 = |\alpha\cos\theta + \beta\cos\theta|^2, \tag{6.6}$$

which is equivalent to (6.4). As the two descriptions are equivalent, it is possible to say that after a rotation of HWP1 and HWP2 of angles θ_1 and θ_2, $|\Psi^{\pm}\rangle$ gets projected after the transmission through the fixed polarizers onto $|2\theta_1 2\theta_2\rangle$.

In the table below the configurations of the half wave plates used for the optimization of the setup and the corresponding projection directions of the state $|\Psi^{\pm}\rangle$ are given; the angles that HWP1 and HWP2 make with the direction of $|H\rangle$ are denoted as θ_1 and θ_2.

The effect of a quarter wave plate is more complicated, as evident from the complex nature of the entries of its matrix. At the angle $\theta = \frac{\pi}{4}$ it turns linearly polarized light in

θ_1 (rad)	θ_2 (rad)	Projection onto
0	0	$\|H\rangle_1 \|H\rangle_2$
$\pi/4$	$\pi/4$	$\|V\rangle_1 \|V\rangle_2$
0	$\pi/4$	$\|H\rangle_1 \|V\rangle_2$
$\pi/4$	0	$\|V\rangle_1 \|H\rangle_2$
$\pi/8$	$\pi/8$	$\|+\rangle_1 \|+\rangle_2$
$-\pi/8$	$-\pi/8$	$\|-\rangle_1 \|-\rangle_2$
$\pi/8$	$-\pi/8$	$\|+\rangle_1 \|-\rangle_2$
$-\pi/8$	$\pi/8$	$\|-\rangle_1 \|+\rangle_2$

Table 1: Projection measurements performed on the entangled state $|\Psi^{\pm}\rangle$ by the combined action of the half-wave plates and the PBSs.

the $|H\rangle$ and $|V\rangle$ directions into circularly polarized light. In the experiment it is placed at a specific angle compared to the direction of propagation of the photon in order to change the phase shift α in state (4.17) to exactly 0 or π to obtain the Bell state $|\Psi^{\pm}\rangle$, as shown in fig. 11. The use of these devices, then, enables us to produce the ideal states to optimize the experimental setup and violate the CHSH inequality.

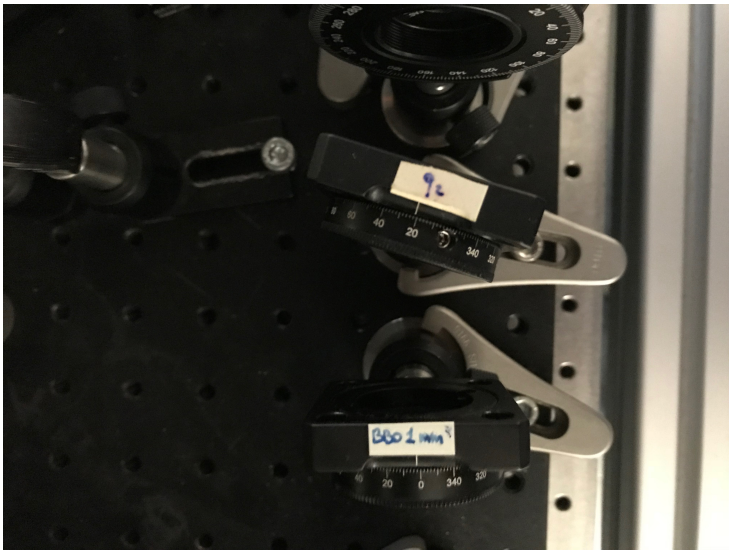

Figure 11: The quarter wave plate (in the middle) placed in the experimental setup between a half wave plate (top) and a BBO crystal (bottom). The angle at which it is placed to obtain the desired phaseshift is found empirically.

6.2 Optimization of the source and back alignment

The optimization of the first part of the experimental setup consists in the optimization of the laser and the alignment of mirrors and lenses, making sure that the beam propagates

horizontally and that it is focused in the right spots: the SHG and the BBO crystals. Since light is visible, it is possible to do this task even while using the protective glasses without the need of any measurement device except the eye.

In the second part, as SPDC light is not visible, even the process of alignment is not trivial. Because of this, the procedure of back alignment was used while only keeping the polarizers, the mirrors, the lenses and the filters in the setup, using the same fibers connected to the SPADs to emit light coming from another laser at 810 nm.

By reconnecting the fibers to the SPADs, one can measure the number of photons accessing the fiber with ≈ 81 ps of resolution at a definite time relative to the trigger, but since the SMF have a core of ≈ 10 μm, it is not easy to focus the light in such a small area with only the back alignment procedure. Because of this, multi mode fibers are used for back alignment and to find the SPDC light.

Once the mirrors are aligned, the BBO crystal is tilted in order to move the position of the intersection of the cones. If the procedure is followed correctly, a peak of Gaussian-like shape as the one shown in fig. 12 in the number of photons will rise at a definite time in at least one of the SPADs. If the peak is found, it can be optimized by slightly moving the focus of the fiber and tilting the mirrors. Once the peak is optimized, if the other is not present, it is useful to do the back alignment procedure again, not changing the conditions of the good path, but trying to make the other beam follow a path as symmetrical as possible to the other. At this point, once reconnected the SPADs, the other peak should

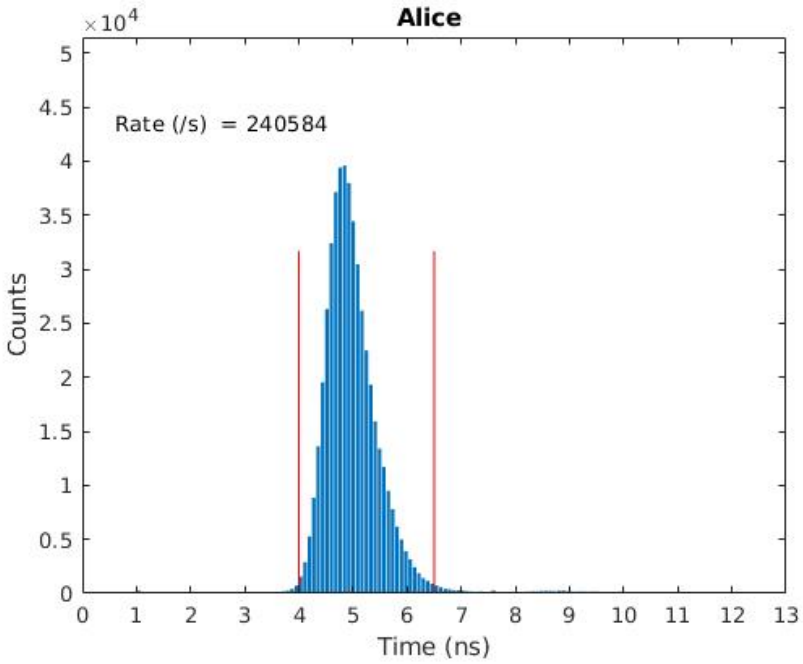

Figure 12: Number of photons detected per second by the SPAD in Alice's path vs. time relative to the trigger (every 13 ns).

be visible, too, making it possible to optimize it. If no peaks show up, back alignment has to be done again, trying to change the directions of the light reflected by the mirrors going directly into the BBO crystal.

When the peaks are found, the same procedure is followed with single mode fibers, with back alignment needed only to focus the beam on the BBO crystal. Once the peaks were optimized with the single mode fibers, more than $2 \cdot 10^5 \ \frac{photons}{s}$ were measured within the peak.

6.3 Finding the instersections of the cones and coincidences

The light measured at this stage is hardly ever the SPDC light in the intersection of the cones showed in fig. 5 (b), as it is probably in the surroundings of the intersections. To make sure that the measured light is the desired one, the two half wave plates HWP1 and HWP2 are placed in the two paths. As extraordinary light is in one cone and ordinary light is in the other, if by rotating the plates of $\frac{\pi}{4}$ the peaks disappear, one has the certainty of not being in the intersection and to be in the (o) cone, corresponding to the direction of the transmission axis of the polarizers.

It is impossible to know *a priori* which part of the cone is seen by the detectors, so that a strategy is necessary to be sure to get in the intersection. The method used can be viewed mathematically as a contraction, bound to converge to the desired point by the *Banach Cacciopoli* lemma.

The first step is to focus only on one path: after twisting the wave plate to get the extraordinary polarized light to be ordinary polarized, one can tilt the mirrors vertically to only effect the height at which the beam arrives at the fiber and see if in one direction the peak appears (this will certainly happen because of how the cones are placed); this way, it will be sure that the other cone is entering the fiber; at this point, noted the direction in which the mirrors were tilted, one can go back and make the peak of the beam decrease to half its original value, consequently compensating the loss by tilting the mirrors horizontally; by rotating the wave plate to its original position, one should see that the beam is less polarized, meaning the intersection of the cones is nearer. By iterating the process, one is bound to end up in the right place.

When both of the beams entering the fibers are unpolarized, the other optical components of the setup are placed and the procedure is done again, since some of the conditions change due to the presence of new optical interactions. The two BBO crystals have to be placed parallel to the other one. To do this, using the notation of the table 1, it is sufficient to check that the coincidences measured in the configurations $|H\rangle_1 |V_2\rangle$ and $|V\rangle_1 |H\rangle_2$ are not influenced by their presence; the same has to be checked with the quarter wave plate. In the meantime, in order to accomplish the phase shift of α in (4.17) to 0 or π, the quarter wave plate has to be tilted as discussed in section 6.1 while checking that the numbers of coincidences in the configurations $|+\rangle_1 |-\rangle_2$ and $|-\rangle_1 |+\rangle_2$ or $|+\rangle_1 |+\rangle_2$ and $|-\rangle_1 |-\rangle_2$ respectively reach an absolute minimum. This time the procedure of alignment is easier, as the intersections are certainly very close to the fibers.

At this point, the last thing to optimize is the number of photons arriving coincidentally at the SPADs. Small differences in the distance run across by the two photons are not significant, thanks to the high speed of light. Non accidental coincidences should already be observable at this point of optimization if the waveplates are placed so that the photons are in states like $|H\rangle_1 |V\rangle_2$ and $|V\rangle_1 |H\rangle_2$. If they are not, it is probably because the two beams entering the fiber are not the ones of the degenerate cones. To avoid this problem, it is always useful to look at the number of coincidences during the procedure described before.

To optimize the number of coincidences, it is useful to work with more states, in order not to get out of the intersections. If, for example, the quarter wave plate is placed to get $|\Psi^-\rangle$ of (1.19), all the configurations of the waveplates to obtain $|H\rangle_1 |V\rangle_2$. $|V\rangle_1 |H\rangle_2$, $|+\rangle_1 |-\rangle_2$ and $|-\rangle_1 |+\rangle_2$ are to be exploited and their coincidences optimized. In the meantime, it is necessary to check that in the configurations $|H\rangle_1 |H\rangle_2$, $|V\rangle_1 |V\rangle_2$, $|+\rangle_1 |+\rangle_2$ and $|-\rangle_1 |-\rangle_2$ the coincidences drop.

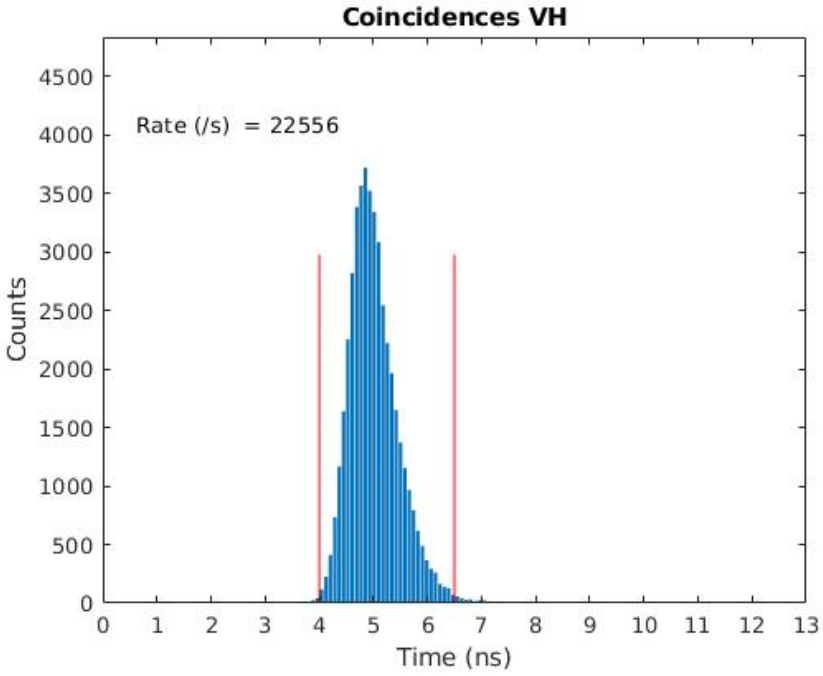

Figure 13: Number of coincidences detected per second vs. time relative to the trigger; measured in the $|V\rangle_1 |H\rangle_2$ configuration.

7 Results

In this sections the results obtained in the experiment are shown.

7.1 Visibility

Once set the quarter waveplate to have $\alpha = \pi$, where α is the phase in (4.17), by calculating the probability of measuring a coincidence in any of the configurations $|H\rangle_1 |H\rangle_2$, $|V\rangle_1 |V\rangle_2$, $|+\rangle_1 |+\rangle_2$ and $|-\rangle_1 |-\rangle_2$, one gets, for example, $p(++) = |\langle +_1 +_2 |\Psi^-\rangle|^2 = 0$, where $\langle +_1 +_2| = \langle +|_1 \langle +|_2$ using the notation of 6.1. The coincidences measured in such configurations, once optimized the setup, should all be accidental. A useful parameter, called *visibility* $\mathcal{V}$ quantifies how significant the quantity of desired coincidences is in comparison with the undesired ones. Taking into consideration the measurements along the (e) and (o) axes,

$$\mathcal{V}_{HV} = \frac{N_{HV} + N_{VH} - N_{HH} - N_{VV}}{N_{HV} + N_{VH} + N_{HH} + N_{VV}}, \tag{7.1}$$

where $N_{HH,VV,HV,VH}$ is the number of coincidences measured in the configurations $|H\rangle_1 |V\rangle_2$. $|V\rangle_1 |H\rangle_2$, $|H\rangle_1 |H\rangle_2$ and $|V\rangle_1 |V\rangle_2$ respectively. Along the diagonal axes,

$$\mathcal{V}_{+-} = \frac{N_{+-} + N_{-+} - N_{++} - N_{--}}{N_{+-} + N_{-+} + N_{++} + N_{--}}. \tag{7.2}$$

The estimated visibilities reached were

$$\mathcal{V}_{HV} = 0.938 \pm 0.001, \tag{7.3}$$
$$\mathcal{V}_{+-} = 0.786 \pm 0.002, \tag{7.4}$$

for the first measure of S ($\alpha = \pi$) and

$$\mathcal{V}_{HV} = 0.959 \pm 0.001, \tag{7.5}$$
$$\mathcal{V}_{+-} = 0.847 \pm 0.001, \tag{7.6}$$

for the second one ($\alpha = 0$). The numbers of coincidences in a given time are distributed according the Poissonian distribution so that their error corresponds to their square root.

7.2 Coincidences and the measurement of S

In order to violate the CHSH inequality (1.16), it is necessary to measure the quantities in the expression $S = \langle a_0 b_0 \rangle + \langle a_0 b_1 \rangle + \langle a_1 b_0 \rangle - \langle a_1 b_1 \rangle$, where $\langle a_x b_y \rangle$ is the average value of the product of the polarization of photon 1 measured along the direction x and the one of photon 2 measured along the direction y, as discussed in sections 1.2.3 and 1.2.4. Recalling section 6.1, to make a measurement of polarization along a certain direction using the setup of this experiment, the half wave plates HWP1 and HWP2 have to be

rotated at determinate angles. The table below displays the angles at which the half wave plates were rotated to violate the CHSH inequality and the corresponding direction of the transmission axes of the two polarizers, labeled with x for photon 1 and y for photon 2:

θ HWP1	θ HWP2	x	y
0	$\frac{\pi}{16}$	$\|H\rangle$	$\cos\frac{\pi}{8}\|H\rangle + \sin\frac{\pi}{8}\|V\rangle$
$\frac{\pi}{4}$	$\frac{5\pi}{16}$	$\|V\rangle$	$-\sin\frac{\pi}{8}\|H\rangle + \cos\frac{\pi}{8}\|V\rangle$
$\frac{\pi}{8}$	$-\frac{\pi}{16}$	$\|+\rangle$	$\cos\frac{\pi}{8}\|H\rangle - \sin\frac{\pi}{8}\|V\rangle$
$-\frac{\pi}{8}$	$\frac{3\pi}{16}$	$\|-\rangle$	$\sin\frac{\pi}{8}\|H\rangle + \cos\frac{\pi}{8}\|V\rangle$

The mean value $\langle a_x b_y\rangle$ can not be measured directly. On the other hand, the coincidences in a certain configuration of the waveplates can be directly measured, making it possible to obtain any desired measurement of $\langle a_x b_y\rangle$ indirectly as

$$\frac{C(\theta_1,\theta_2)+C(\theta_1^\perp,\theta_2^\perp)-C(\theta_1,\theta_2^\perp)-C(\theta_1^\perp,\theta_2)}{C(\theta_1,\theta_2)+C(\theta_1^\perp,\theta_2^\perp)+C(\theta_1,\theta_2^\perp)+C(\theta_1^\perp,\theta_2)}, \tag{7.7}$$

where θ_1 and θ_2 are the directions of the polarizations of photons 1 and 2 after the passage through the wave plates and $\theta_1^\perp$ and $\theta_2^\perp$ are the orthogonal directions; $C(\cdot,\cdot)$ is the number of coincidences measured given these two directions. To obtain the results, then, all of the 16 configurations of the wave plates using the angles in the table above have to be used. It would be ideal to measure θ_i and $\theta_i^\perp$ simultaneously with the use of two more detectors to count directly the reflected photons from the beam splitters. This requires the assumption that the state from the source is independent of the analyzer settings [8].

The first set of measurements was taken with phase shift α in (4.17) set to π. The angles made by Alice's waveplate are 0, $\frac{\pi}{4}$ and $\pm\frac{\pi}{8}$, corresponding to the notation a_0, $a_0^\perp$, a_1 and $a_1^\perp$ respectively. The ones made by Bob's waveplate are Alice's rotated by $\frac{\pi}{16}$ and will be denoted as b_0, $b_0^\perp$, b_1 and $b_1^\perp$. The coincidences measured are given in the table below:

	x	0	0	1	1
y		a_0	$a_0^\perp$	a_1	$a_1^\perp$
0	b_0	5028 ± 70	22304 ± 150	5459 ± 70	24274 ± 160
0	$b_0^\perp$	23213 ± 150	7601 ± 90	23765 ± 150	5128 ± 71
1	b_1	4733 ± 70	22969 ± 150	16060 ± 130	4824 ± 70
1	$b_1^\perp$	25744 ± 160	6261 ± 80	11230 ± 110	19187 ± 140

giving a measure of S of

$$|S| = 2.295 \pm 0.007. \tag{7.8}$$

The measurement was made again while placing the quarter wave plate to get $\alpha = 0$, and therefore using the state $|\Psi^+\rangle$ of (1.19). To establish the notation used, this time, making x correspond to $\theta_1 = 0$, $\frac{\pi}{4}$ with labels 0 and 1 respectively and y correspond to $\theta_2 = -\frac{\pi}{8}$ and $\frac{\pi}{8}$ again labeled as 0 and 1 respectively, it is possible to show that $\langle a_0 b_0\rangle = \langle a_0 b_1\rangle = \langle a_1 b_0\rangle = -\langle a_1 b_1\rangle = -\frac{1}{\sqrt{2}}$. The inequality (1.16) holds without change in notation, then. The coincidences measured are given in the table below:

	x	0	0	1	1
y		a_0	$a_0^\perp$	a_1	$a_1^\perp$
0	b_0	6858 ± 80	20629 ± 140	2558 ± 50	19579 ± 140
0	$b_0^\perp$	14794 ± 120	4176 ± 60	11749 ± 100	2255 ± 50
1	b_1	2664 ± 50	15740 ± 130	20446 ± 140	5122 ± 70
1	$b_1^\perp$	9311 ± 100	7742 ± 90	2538 ± 50	19830 ± 140

Giving a measure of S of

$$|S| = 2.35 \pm 0.01. \tag{7.9}$$

7.3 Conclusions

The results both violate the inequality (1.16), (7.8) within 42σ and (7.9) within 35σ, violating the locality constraint (1.10). The experiment relies on very few assumptions and still gives the predicted results. The source is proven to be optimized, since it produces photons that show entangled features. With a $3W$ mode-locked laser, producing a pulse every $13ns$, it was possible to measure up to more than $2 \cdot 10^5$ $\frac{photons}{s}$ per SPAD with $\approx 10\%$ of them being coincident, in single mode fibers. The optimization procedure has proven to be successful, even though the results obtained are not strictly the optimal ones. It is clear that our measures of S are not compatible with the expected value of (1.18), and this has to be because of the imperfect optimization of the wave function of the photons entering the detectors. The states used are not exactly $|\Psi^-\rangle$ and $|\Psi^+\rangle$ of (1.19), probably due to slight problems in the alignment of the two BBO crystals and in the alignment of the mirrors. The visibilities are lower than expected and some asymmetries can be seen in the collected data, suggesting that the photons entering the SPADs do not belong strictly to the intersections of the cones of the SPDC light.

Despite that, the optical devices are placed and aligned, making it possible to replicate the experiment at any given time making very few adjustments. The entangled pairs produced by the source can now be easily measured and the setup is fixed and will be able to measure coincidences in the immediate and possibly in the distant future, enabling it to be integrated with new parts to entangle the photons in more degrees of freedom, creating situations of hyperentanglement.

This page intentionally left blank

8 Bibliography

[1] A. Einstein, B. Podolsky, and N. Rosen. Can quantum-mechanical description of physical reality be considered complete? *Phys. Rev., 47, May 1935*

[2] John S. Bell. On the Einstein Podolsky Rosen paradox. *Physics*, 1(3), 195-200

[3] Christopher G. Gerry and Peter l. Knight. Introductory Quantum Optics. *Cambridge University Press*, chapter 9

[4] N. Brunner, D. Cavalcanti, S. Pironio, V. Scarani, S. Wehner. Bell Nonlocality. *Reviews of Modern Physics, Volume 86, April-June 2014,* section I,A

[5] B. E. A. Saleh, M.C. Teich. Fundamentals of Photonics. *Wiley-Interscience. A John Wiley & Sons, Inc., Publication*, chapters 2, 3, 6, 9, 14, 15 and 21.

[6] Adrian C. Melissinos. Principles of Modern Technology. *Cambridge University Press*, chapter 4.8, 4.9 and 4.10.

[7] Mark Fox. Quantum Optics - an Introduction. *Oxford University Press, 2006*, chapter 4

[8] Paul G. Kwiat, Klaus Mattle, Harald Weinfurter, and Anton Zeilinger. New High Intensity Source of Polarization-Entangled Photon Pairs. *Phys. Rev. 75, December 1995*

[9] Giuseppe Vallone and Paolo Mataloni. Generation and Applications of n-Qubit Hyperentangled Photon States. *Advances in Atomic, Molecular, and Optical Physics, Volume 60,* chapter 6, section 3

[10] Stephen M. Barnett. Quantum Information. *Oxford University Press, 2009*, chapter 3.3.